J. metamorphic Geol., 1993, **11**, 357–370

Calculated fluid evolution path versus fluid inclusion data in the COHN system as exemplified by metamorphic rocks from Rogaland, south-west Norway

R. J. BAKKER AND J. B. H. JANSEN
Department of Geochemistry, Institute for Earth Sciences, Budapestlaan 4, PO Box 80.021, 3508 TA Utrecht, The Netherlands

ABSTRACT Fluid evolution paths in the COHN system can be calculated for metamorphic rocks if there are relevant data regarding the mineral assemblages present, and regarding the oxidation and nitrodation states throughout the entire P–T loop. The compositions of fluid inclusions observed in granulitic rocks from Rogaland (south-west Norway) are compared with theoretical fluid compositions and molar volumes. The fluid parameters are calculated using a P–T path based on mineral assemblages, which are represented by rocks within the pigeonite-in isograd and by rocks near the orthopyroxene-in isograd surrounding an intrusive anorthosite massif. The oxygen and nitrogen fugacities are assumed to be buffered by the coexisting Fe–Ti oxides and Cr-carlsbergite, respectively. Many features of the natural fluid inclusions, including (1) the occurrence of CO_2–N_2-rich graphite-absent fluid inclusions near peak M2 metamorphic conditions (927° C and 400 MPa), (2) the non-existence of intermediate ternary CO_2–CH_4–N_2 compositions and (3) the low-molar-volume CO_2-rich fluid inclusions (36–42 $cm^3\,mol^{-1}$), are reproduced in the calculated fluid system. The observed CO_2–CH_4-rich inclusions with minor N_2 (5 mol%) should also include a large proportion of H_2O according to the calculations. The absence of H_2O from these natural high-molar-volume CO_2–CH_4-rich inclusions and the occurrence of natural CH_4–N_2-rich inclusions are both assumed to result from preferential leakage of H_2O. This has been previously experimentally demonstrated for H_2O–CO_2-rich fluid inclusions, and has also been theoretically predicted. Fluid-deficient conditions may explain the relatively high molar volumes, but cannot be used to explain the occurrence of CH_4–N_2-rich inclusions and the absence of H_2O.

Key words: COHN system; fluid evolution; fluid inclusions; re-equilibration; Rogaland.

INTRODUCTION

The evolution of fluids in metamorphic terranes can be traced by accurate measurement of the composition and density of fluid inclusions. The trapping sequence of different generations of inclusions can be established from their geometrical relationships. Each generation represents distinct metamorphic fluids, which only mix locally at intersections. The fluids are often composed of gas species in the COHN system. Nitrogen has been frequently analysed from rocks and minerals by mass spectrometry. This method entails rock-crushing and mineral-cleaving under a vacuum and is non-selective. The *in situ* measurement of N_2 in fluid inclusions by non-destructive methods was first described by Dhamelincourt *et al.* (1979), Swanenberg (1980) and Guilhaumou *et al.* (1981) using microthermometry and Raman spectroscopy. The composition of metamorphic fluids in the COHN system may of course be influenced by mineral assemblages present in the host rock, and these in turn are dependent on the conditions of metamorphism (Bastoul *et al.*, 1991; Doria *et al.*, 1991). Metamorphic P–T paths derived from geothermometry and geobarometry of stable mineral assemblages can be used to calculate the coexisting fluid compositions. The results thus obtained can then be compared with those from natural fluid inclusions. In order to carry out these calculations, several fundamental assumptions must be made. First, the fluid compositions are defined by the P–T conditions and internal nitrogen- and oxygen- or hydrogen-fugacity buffers. Second, carbon, oxygen, hydrogen and nitrogen must remain available in the rock at all P–T conditions. The presence of minerals containing these elements, which take part in chemical equilibria, allows their interchange with the fluid phase.

The original source of nitrogen in sedimentary rocks is most often assumed to be organic matter (Arrhenius, 1950; Stevenson, 1962). Stevenson (1962) postulated that most nitrogen exists as ammonium ions held within mineral lattices. In metamorphic and magmatic rocks ammonium substitutes for potassium in biotite, muscovite, K-feldspar and plagioclase (Stevenson, 1962; Hallam & Eugster, 1976; Honma & Itihara, 1981; Touret, 1982; Duit *et al.*, 1986; Bos *et al.*, 1988). Dubessy & Ramboz (1986) described the behaviour of N_2 fluids that originated from the release of ammonium from minerals during diagenesis and metamorphism.

In order to calculate fluid compositions within the COHN system, we have developed a *PASCAL* computer

program (Bakker & Jansen, 1991a; Bakker, 1992). Using this program it is possible to calculate the P–T–V–X relations of both pure gases and gas mixtures, from the relevant equations of state, and data on molar volumes, isochoric systems and solvi (Holloway & Reese, 1974; Holloway, 1977; Flowers, 1979; Jacobs & Kerrick, 1981; Kerrick & Jacobs, 1981; Saxena & Fei, 1987). Thermodynamic data on gases and mineral buffers were taken from several sources: Eugster & Skippen (1967), JANAF (1971), Robie *et al.* (1978) and Berman (1988). Six independent gas reactions (Eqs 1–6) are used to calculate fugacities of the nine relevant gas species (O_2, H_2, N_2, H_2O, CO_2, CO, CH_4, NH_3, NO_2), according to the method described by French (1966):

$$C + O_2 \rightleftharpoons CO_2, \quad (1)$$

$$C + \tfrac{1}{2}O_2 \rightleftharpoons CO, \quad (2)$$

$$C + 2H_2 \rightleftharpoons CH_4, \quad (3)$$

$$H_2 + \tfrac{1}{2}O_2 \rightleftharpoons H_2O \quad (4)$$

$$\tfrac{1}{2}N_2 + \tfrac{3}{2}H_2 \rightleftharpoons NH_3, \quad (5)$$

$$\tfrac{1}{2}N_2 + O_2 \rightleftharpoons NO_2. \quad (6)$$

The total pressure of the fluid is given by Dalton's law:

$$P_{\text{total}} = \sum \left(\frac{f_i}{\gamma_i}\right), \quad (7)$$

in which P_{total}, f_i and γ_i are the total fluid pressure, fugacity and fugacity coefficient of gas species i, respectively. The total fluid pressure is assumed to be equal to the lithostatic pressure, although this need not be the case (Lamb & Valley, 1985; Skippen & Marshall, 1991). In addition, two equations are needed to define all gas fugacities at given P–T conditions. These two equations are given by mineral buffers that define fugacities of two distinct gas species.

OXIDATION AND NITRODATION TRENDS IN ROCKS

Mineral assemblages in metamorphic rocks are capable of buffering the concentration of volatile species in metamorphic fluids (Greenwood, 1975). An inventory of fluids in various metamorphic rocks by Rice & Ferry (1982) indicates that in comparison with infiltration, buffering is, in general, a far more important control on fluid composition. If infiltration of an external fluid occurs, the local pore fluid composition may still be controlled by the buffering capacity of the rock (Rice & Ferry, 1982) until the buffering reaction is exhausted.

The oxidation state of a rock may be described by buffer reactions, whose components are not necessarily present in the rock (Haggerty, 1976). For example, the top of the upper mantle is as oxidized as the quartz–fayalite–magnetite (QFM) buffer (Saxena, 1989). The oxygen fugacity of the lower upper mantle is closer to the WI buffer (Ulmer *et al.*, 1987). Holloway (1981) characterized a hypothetical metamorphic fluid without reference to data on coexisting mineral assemblages. His oxygen fugacities are expressed in terms of their position relative to the QFM buffer. In general, the oxidation state of the lower and upper crust, with relatively well-known phase relations, can be established using a single reaction (Thompson, 1975; Thompson & Thompson, 1976; Ferry, 1979; Ferry & Burt, 1982). Coexisting Fe–Ti oxides (Eq. 8) have been used to estimate temperatures from several igneous and high-grade metamorphic rocks (Buddington & Lindsey, 1964; Spencer & Lindsey, 1981), using the reaction

$$3Fe(Ti, Fe)O_3 \rightleftharpoons 2Fe_2(Ti, Fe)O_4 + O_2. \quad (8)$$

The compositions of these phases at equilibrium are dependent upon temperature and oxygen fugacity. Therefore, temperature estimates can be used to indicate the oxidation state of these rocks. Here, coexisting Fe–Ti oxides (Eq. 8) are used to calculate the reference oxygen fugacities within the rocks. Lamb & Valley (1985) and Valley *et al.* (1990) have also used coexisting Fe–Ti oxides (Eq. 8) to calculate local oxygen fugacities in granulites. They used several mineral buffers, assuming ideal stoichiometry, to calculate H_2O fugacity in pelites (Eqs 9 & 10) and amphibolites (Eq. 11):

$$2KFe_3(AlSi_3)O_{10}(OH)_2 + O_2 \rightleftharpoons 2KAlSi_3O_8 + 2Fe_3O_4 + 2H_2O, \quad (9)$$

$$KAl_2Si_3AlO_8(OH_2) + SiO_2 \rightleftharpoons Al_2SiO_5 + KAlSi_3O_8 + H_2O, \quad (10)$$

$$Ca_2Mg_5Si_8O_{22}(OH)_2 \rightleftharpoons 2CaMgSi_2O_6 + 3MgSiO_3 + SiO_2 + H_2O. \quad (11)$$

An oxygen buffer with higher capacity (Eq. 12) than from coexisting Fe–Ti oxides (Eq. 8) can also be used to calculate oxygen fugacities for charnockites at granulitic conditions (Hansen *et al.*, 1984):

$$6FeSiO_3 + O_2 \rightleftharpoons 2Fe_3O_4 + 6SiO_2. \quad (12)$$

Within the COHN system, an extra buffer is needed to define the nitrogen fugacity. Hallam & Eugster (1976) estimated equilibrium constants for reactions involving the ammonium silicates tobelite and buddingtonites:

$$6NH_4Si_3AlO_8(\tfrac{1}{2}H_2O) \rightleftharpoons 2NH_4Al_2Si_3AlO_{10}(OH)_2 + 12SiO_2 + 4NH_3 + 3H_2O, \quad (13)$$

$$2NH_4Si_3AlO_8(\tfrac{1}{2}H_2O) \rightleftharpoons Al_2SiO_5 + 5SiO_2 + 2NH_3 + 2H_2O. \quad (14)$$

However, the accuracy of their equilibrium constant estimates is not good. Voncken *et al.* (1988) argued against the existence of natural hydrous buddingtonite. They measured the unit-cell parameters of synthetic anhydrous buddingtonite and found these to be similar to the natural supposed hydrous samples. Hallam & Eugster (1976) suggested that ammonium takes part in a cation exchange reaction with muscovite:

$$\text{K-muscovite} + NH_4^{+(aq)} \rightleftharpoons NH_4\text{-muscovite} + K^{+(aq)}. \quad (15)$$

Bos (1990) estimated the distribution coefficient of NH_4^+/K^+ between phlogopite and a chloride vapour phase, analogous to Eq. (15). Preliminary calculations using Eq. (14) indicate that nitrogen is an important gas species in the fluids at high temperatures.

Because of the incomplete and imprecise thermodynamic data, we have used N_2-rich natural fluid inclusions to select an appropriate nitrogen buffer from which to calculate the nitrodation trend. The nitrodation trend is displayed relative to the Cr-carlsbergite buffer (Eq. 16), analogous to the method described by Holloway (1981) for oxygen fugacities:

$$2Cr + N_2 \rightleftharpoons 2CrN. \quad (16)$$

ROGALAND (SOUTH-WEST NORWAY)

The method was tested against natural fluid inclusion data from the metamorphic rocks of Rogaland, south-west Norway (Fig. 1), which have been the subject of many previous studies (Hermans *et al.*, 1975; Sauter, 1983; Jansen *et al.*, 1985; Tobi *et al.*, 1985; Maijer & Padget,

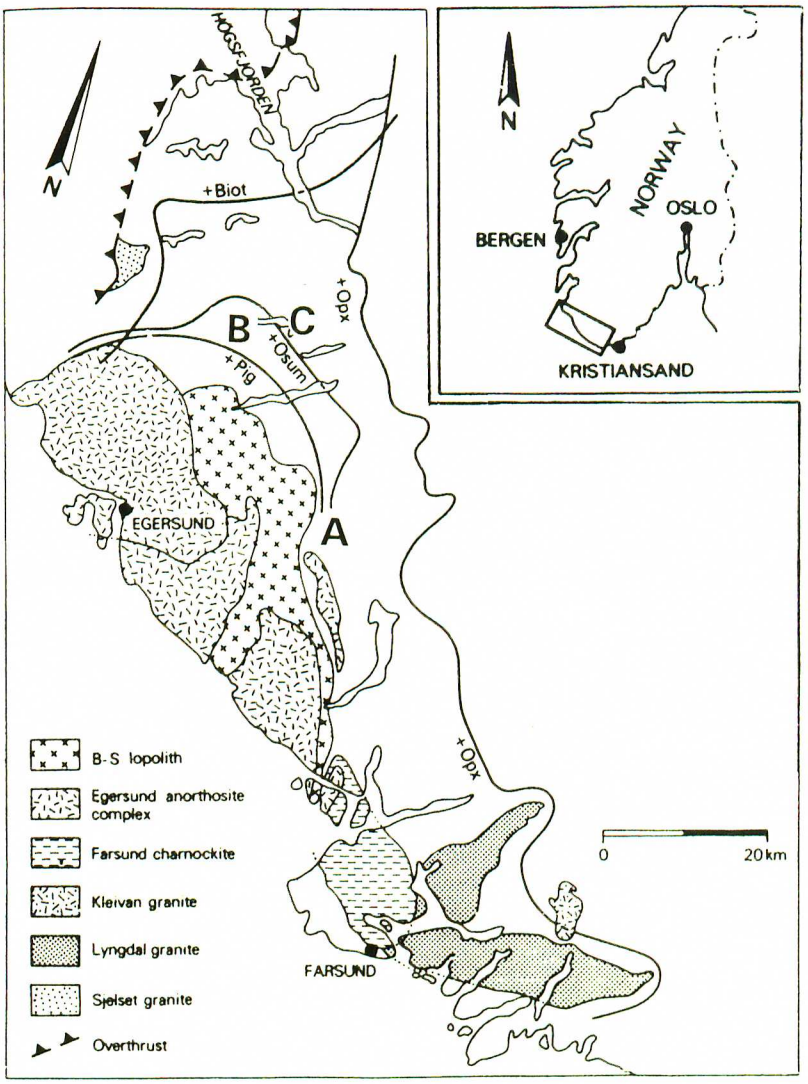

Fig. 1. Isograd map of Rogaland, south-west Norway (after Jansen *et al.*, 1985). The locations of rocks used by Swanenberg (1980) and van den Kerkhof *et al.* (1991) for fluid inclusion measurements are indicated by A (Drangsdalen), B (Austrumdalsvatnet) and C (Faurefjell metasediments). The pigeonite-in, osumulite-in, hypersthene-in and biotite-in isograds are indicated with +Pig, +Osum, +Opx and +Biot, respectively.

1987; Bol, 1990). Three stages of Grenvillian metamorphism (M1–M3) and a Caledonian stage (M4) have been recognized (Table 1 & Fig. 2) within the migmatitic complex enveloping the Egersund anorthositic complex and the Bjerkreim–Sokndal lopolith (Duchesne *et al.*, 1985).

Table 1. Metamorphic grade, age and setting of metamorphism recorded in Rogaland, south-west Norway (after Hermans *et al.*, 1975; Jansen *et al.*, 1985; Tobi *et al.*, 1985).

Metamorphic grade		Age (Ma)	Setting
M1	Upper amphibolite to granulite	1200	Regional metamorphism
M2	Granulite (high T, intermediate P)	1050	Thermal overprint, induced by intrusion of leuconoritic phase of lopolith
M3	Medium grade	970–870	Retrograde metamorphism during slow, nearly isobaric cooling
M4	Prehnite–pumpellyite to greenschist	400	Caledonian orogeny, overthrusting

The precise relationships between the migmatic, metamorphic and tectonic events in this area have not yet been established, although several deformation phases have been distinguished (Hermans *et al.*, 1975; Huijsmans *et al.*, 1981). The earliest phase of isoclinal folding, D1, is presumed to be coeval with migmatization during M1. Basic intrusions, post-dating this migmatization, are deformed by the main phases of deformation (D2–D3). These deformation phases affected the basal parts of the Bjerkreim–Sokndal lopolith (Fig. 1), which was intruded during low-P granulite facies M2 metamorphism (Pasteels *et al.*, 1979; Wielens *et al.*, 1981). Huijsmans *et al.* (1981) have suggested that a long period of intense ductile deformation (D2) was coeval with the high-T metamorphic (M2) events, with deformation behaviour becoming more brittle (D3) at the intermediate temperatures of M3.

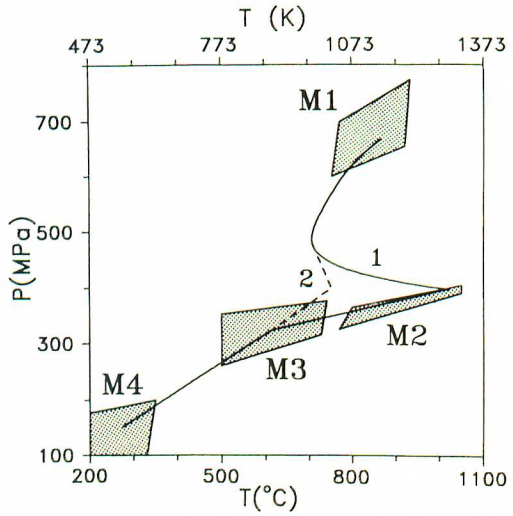

Fig. 2. Estimated P–T conditions for each of the metamorphic events (after Bol, 1990) described in Table 1. The supposed uplift path 1 (solid line) is used for the fluid calculations in rocks within the pigeonite-in isograd with a maximum temperature of 1020° C. Path 2 (dashed line) indicates a typical P–T development for rocks near the orthopyroxene-in isograd with a maximum temperature of 750° C during M2. Both paths are proposed to have equal pressures during M2 at different peak temperatures. Equal denudation rates result in a simultaneous comparable pressure development.

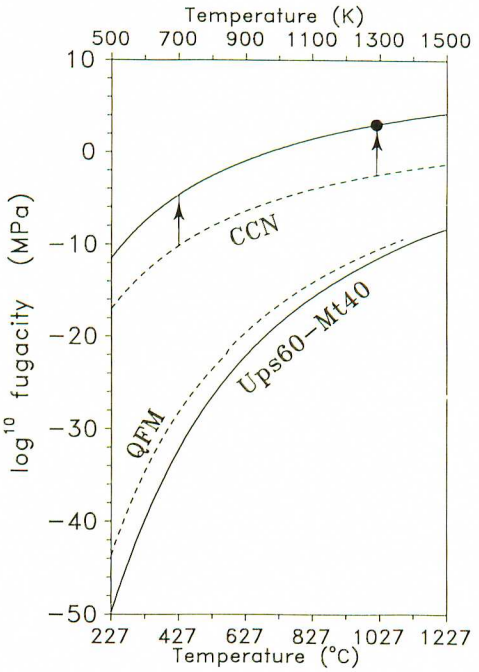

Fig. 3. Temperature–$\log_{10}$ (fugacity) diagram for calculated nitrogen and oxygen fugacities (in MPa). The Cr-carlsbergite buffer (CCN; dashed line) is shifted +5.5 $\log_{10}$ units (solid line) to obtain the nitrogen fugacity of pure N_2 fluid inclusions at near peak M2 conditions (closed circle). Coexisting Fe–Ti oxides (Ups60–Mt40; solid line) defines the oxygen fugacity. The quartz–fayalite–magnetite buffer (QFM; dashed line) indicates the relatively reduced nature of the Ups60–Mt40 buffer.

Jansen *et al.* (1985) successfully used several geothermobarometers in combination with isograd mapping (pigeonite-in, osumulite-in, hypersthene-in and biotite-in isograds, see Fig. 1) and age determinations to unravel the polymetamorphic evolution of this area. Coexisting magnetite–ulvospinel and hematite–ilmenite solid solutions (Eq. 8) were applied as a geothermometer and oxygen barometer for the M2 and M3 events (Duchesne, 1970). A best fit through the data (fig. 10 in Jansen *et al.*, 1985) within a T–f_{O_2} diagram coincides with the 60% ulvospinel line, which is used to indicate the oxygen fugacity of the rock at temperatures between 227 and 1227° C (Fig. 3). This is somewhat more reduced than the QFM buffer, which is also shown in Fig. 3. Resetting of this geothermometer at low P–T, as argued by Frost & Chacko (1989), results in underestimates of the peak metamorphic conditions, but does not, however, influence our fluid calculations. The P–T paths (1 & 2 in Fig. 2), which are used as a basis for calculation of fluid compositions and molar volumes, are assumed to be representative of these rocks by Bol (1990).

There are no available data concerning the natural N_2 buffering in rocks of this area: a few ammonium analyses reveal up to 55 ppm in metasedimentary biotite. The dot in Fig. 3 indicates the nitrogen fugacity (1021 MPa) in pure N_2 fluid inclusions at peak M2 conditions. The calculated nitrogen fugacity from the Cr-carlsbergite buffer (Eq. 16) is shifted 5.5 $\log_{10}$ units (CCN + 5.5) to obtain the same fugacity (Fig. 3).

A fluid inclusion study of the rocks in the Rogaland area was undertaken by Swanenberg (1980), who used microthermometry (Table 2) and gas chromatography (Table 3) to obtain density and compositional data. His measurements are recalculated to molar fractions and molar volumes of single fluid inclusions. He optically identified six types, of which only the carbonic, the biphase H_2O–CO_2, the CH_4-rich and the N_2-rich fluid inclusions are considered here. In general, aqueous fluid inclusions have lower molar volumes than gaseous inclusions. Within a zone of about 10 km around the Bjerkreim–Sokndal lopolith, the average H_2O content in fluid inclusions seems to be significantly lower (47 vol.%) than in the lower-grade metamorphic areas (72 vol.%) further from the contact. Swanenberg (1980) believed that the carbonic fluid inclusions represented the dominant fluid phase present during peak granulite metamorphism (M2), but that measurements of their densities only partly reflect this condition. An N_2-rich fluid must have been trapped in an 'early secondary' stage, following emplacement of the carbonic fluids. Low-density carbonic fluid inclusions result from partial decrepitation or fluid deficiency (Swanenberg, 1980; Bol, 1990) during peak M2 metamorphic conditions. High-density carbonic and N_2 fluid inclusions (Table 2) strongly suggest post-entrapment re-equilibration of pre-existing fluid inclusions to high densities during retrograde near-isobaric cooling. An early origin (M1) for high-density CO_2-rich fluids is considered unlikely, because the host minerals may be expected to have recrystallized

Table 2. Volume% H_2O, compositions (mol%), densities (g cm^{-3}) and molar volume (cm^3 mol^{-1}) of four types of fluid inclusions, deduced from microthermometrical data, identified by Swanenberg (1980). Density and molar volume is occasionally specified for several locations (Dr = Drangsdalen, Fa = Faurefjell metasediments indicated with A and B in Fig. 1 respectively). Based upon composition, the N_2-rich, the CH_4-rich and the CO_2–H_2O are divided into three, two and two groups, respectively.

Fluid inclusion type	Volume% H_2O (room temperature)	Non-aqueous phase		Molar volume	Special remarks
		Composition	Density		
Carbonic	0	CO_2 52–100 N_2 48–0	Dr = 0.89 Fa = 1.03–1.07 range = 0.70–1.23	Dr = 49 Fa = 41–43 range = 36–63	Critical homogenization of CO_2 phase at −37° C, (additional N_2 up to 48 mol%). In graphite-bearing rocks additional CH_4.
N_2-rich	0–80	(a) N_2 10–96 CO_2 90–4			Maximally 55 vol% solid CO_2 at −170° C in fi.s *k*.
		(b) N_2 96–100 CO_2 4–0	(b) Dr > 0.78 range = 0.53–0.63	(b) Dr < 36* range = 44–52 (b) Dr < 20† range = 22–26	
		(c) N_2 80–100 CH_4 20–0			
CH_4-rich	(a) 0–30	(a) CH_4 100	(a) 0.03–0.04	(a) 400–533* (a) 54–56†	Fluid inclusions (a) have well-developed negative crystal shape.
	(b) 0	(b) CH_4 100	(b) 0.20–0.25	(b) 64–80	
CO_2–H_2O	(a) 60–90	(a) CO_2 100	(a) 0.6–0.69	(a) 19–26†	CO_2 gas phase is occasionally contaminated with N_2.
	(b) 0–90	(b) CO_2 100	(b) 0.6–0.9	(b) 19–40†	Fluid inclusions (b) in cluster-like configuration or in trails have positive correlation between T_H of the CO_2 phases and vol.% H_2O, and originated from an unmixed fluid.

* Molar volume with maximum amount of H_2O.
† Molar volume with minimum amount of H_2O.

during the extremely high temperatures of the M2 stage. Mixing of a late-stage aqueous fluid with fluid from decrepitated fluid inclusions resulted in cluster-like arrangements of carbonic and H_2O–CO_2 or H_2O–N_2 fluid inclusions (Swanenberg, 1980).

Raman spectrometry on gaseous fluid inclusions from the area (Table 3) were undertaken by van den Kerkhof *et al.* (1991). This confirmed the presence of N_2 and CH_4 in most quartz samples obtained from the metasediments enveloping the Bjerkheim–Sokndal lopolith and from Egersund anorthosite complex. Three compositional groups of gaseous, non-aqueous fluid inclusions were recognized: (1) CO_2–N_2 mixtures with 0–3 mol% CH_4, (2) CO_2–CH_4 mixtures with <10 mol% N_2 and (3) N_2–CH_4

Table 3. Composition (mol%) and molar volume (V_M, cm^3 mol^{-1}) of gaseous fluid inclusions from three locations in Rogaland (A, B and C in Fig. 1), for two analytical techniques: bulk gas chromatography without information on H_2O (Swanenberg, 1980) and Raman spectrometry on individual fluid inclusions that are larger than 10 μm in diameter (van den Kerkhof *et al.*, 1991). Sample numbers were used by van den Kerkhof *et al.* (1991) are indicated. Sample 191 is divided into H1 and H3 fluid inclusions.

		A (Drangsdalen) Amphibole leuconorite		B (Asheim/Snøsvatnet) Faurefjell metasediments	C (Austrumdalsvatnet) Graphite-bearing granetiferous migmatite	
Gas chromatography	CO_2	45.8		28.6–83.3	1.0–8.7	
	CH_4	—		0.1–0.4	44.8–48.7	
	N_2	54.2		16.4–71.4	42.6–54.6	
Raman spectrometry	Sample	191 (H3 type)	191 (H1 type)	250	306	311
	CO_2	89–94	0–1	58–100	0–62	1–32
	CH_4	0–3	1–2	—	29–100	7–92
	N_2	5–7	97–98	0–42	0–10	5–91
	H_2O	+	—	±	±	±
	Graphite	—	—	—	+	+
	V_M	45–75	50–90	45–55	54–75	48–60

mixtures with <10 mol% CO_2. The first group (CO_2–N_2-rich), with molar volumes of between 50 and 55 $cm^3\ mol^{-1}$, found in the Faurefjell metasediments (Table 3), are assumed by van den Kerkhof *et al.* (1991) to be the first generation. Several post-entrapment re-equilibration mechanisms have been used to explain the composition and molar volume changes. Diminution of the inclusion volume and partial decrepitation during post-entrapment isobaric cooling may explain higher (up to 90 $cm^3\ mol^{-1}$) and lower molar volumes (down to 45 $cm^3\ mol^{-1}$) of the CO_2–N_2-rich and CO_2 fluid inclusions (van den Kerkhof *et al.*, 1991). They propose late-stage H_2 diffusion into fluid inclusions, demonstrated experimentally in quartz by Hall *et al.* (1989), resulting in the formation of CH_4. The CO_2 then reacts with CH_4 to form the more stable graphite and H_2O phases. Thus, the composition and density of fluid inclusions is controlled by H_2 diffusion through the crystal. Therefore, a mineral assemblage buffering the H_2 fugacity may well be controlling the fluid density and composition in apparently isolated and closed fluid inclusions.

FLUID EVOLUTION CALCULATION

COH system

Calculations of fluid character are confined to the COH system owing to the probably limited occurrence of nitrogen in fluids, micas and feldspars. Rocks within the pigeonite-in isograd surrounding the Bjerkreim–Sokndal lopolith and the Egersund anorthosite complex (Fig. 1) have suffered three metamorphic stages, M1, M2 and M3. *P–T* path 1 (Fig. 2) is used to calculate fluid compositions and molar volumes. Stable fluid compositions and graphite boundaries shift for the differing conditions of M1, M2 and M3, as illustrated in Fig. 4 at 865° C and 669 MPa, 1019° C and 400 MPa, and 614° C and 323 MPa. At M1 conditions (Fig. 4a), a CO_2-rich fluid is in equilibrium with graphite, which may precipitate from the fluid on to grain boundaries or within cracks. At M2 conditions (Fig. 4b), the activity of carbon in the fluid is <1, and graphite is unstable. Any graphite accessible to the circulating buffered fluid will react totally to form CO_2 and CO. At M3 conditions (Fig. 4c), the fluid is rich in CH_4 and once again in equilibrium with graphite.

The COH diagrams in Fig. 4 present fluid compositions at fixed *P–T* conditions, and do not show the fluid evolution. Furthermore, the exact composition of the fluid cannot be deduced from these diagrams. The proposed retrograde metamorphic *P–T* paths (Fig. 2) indicate a continuous decrease in pressure with time. Therefore, we have chosen a pressure versus fluid composition plot (Fig. 5) to present the fluid evolution. During M1 the fluid varies in composition from a CO_2-rich fluid at 669 MPa to an H_2O-rich fluid with minor and equal amounts of CO_2 and CH_4 at the lower-pressure boundary of this metamorphic stage (614 MPa). H_2O remains the major fluid component between M1 and M2, with a minor amount of CH_4. Increasing temperatures during M2 led once again to a CO_2-rich fluid. At peak metamorphic

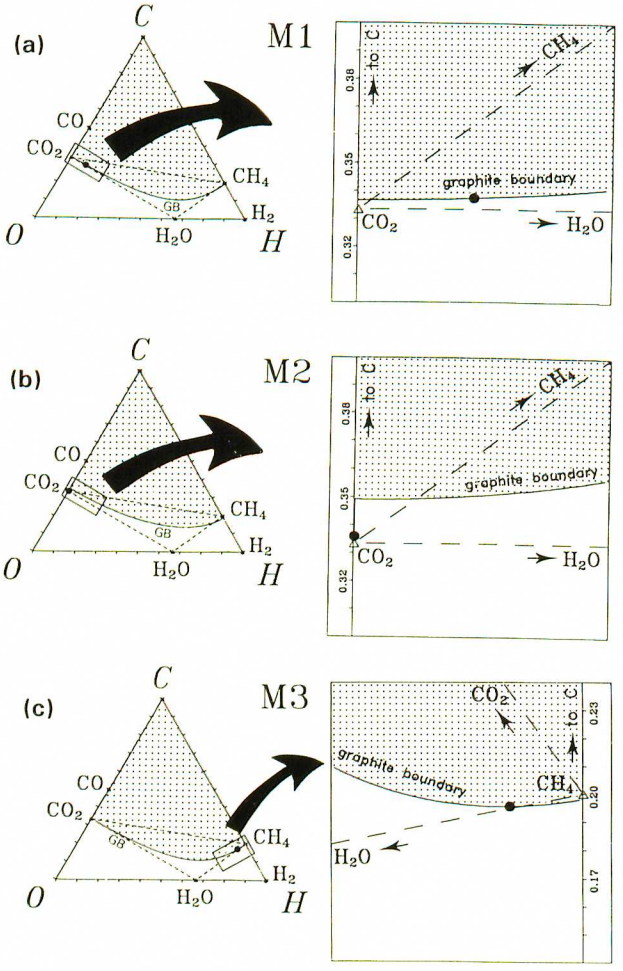

Fig. 4. COH diagrams for (a) the M1, (b) M2 and (c) M3 metamorphic events. The graphite boundary is indicated with a curved solid line. Stable fluid compositions do not occur in the shaded area. The small rectangles within the COH triangular diagrams are enlarged to square diagrams, in which the vertical axis is stretched to emphasize the position of the graphite boundary with respect to the CO_2–CH_4 tie-line. The closed circle represents the calculated fluid compositions for each metamorphic phase.

conditions during M2, between 427 and 359 MPa, graphite is no longer stable (the carbon activity is <1). The fluid composition is CO_2-rich with minor amounts of CO (not represented in Fig. 5), whereas the molar fractions of CH_4 and H_2O are zero. During M3 the fluid evolved from an H_2O-rich fluid with equal and minor amounts of CH_4 and CO_2 at 345 MPa to a CH_4-rich fluid at 266 MPa. Finally, at M4 conditions, the fluid remains CH_4-rich.

COHN system

Calculations of fluid character were also undertaken for the expanded COHN system. This system has been described with regard to the Rogaland area by Swanenberg (1980). He describes N_2-rich fluid inclusions post-dating

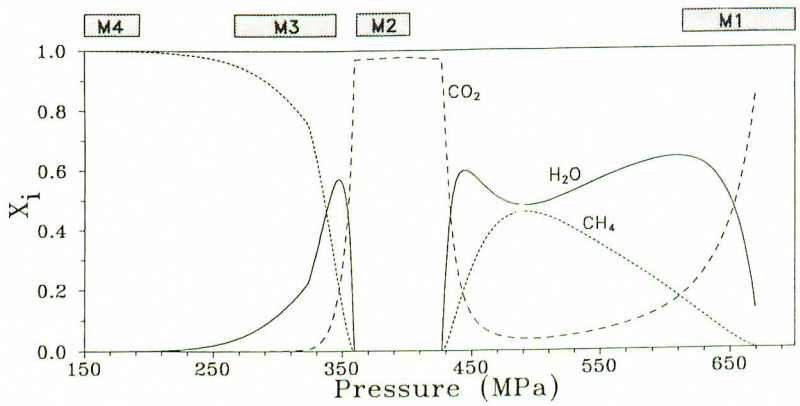

Fig. 5. P–X_i (molar fraction) diagram for the gas species H_2O (solid line), CH_4 (stippled line) and CO_2 (dashed line). P–T conditions of path 1 (Fig. 2) are used to calculate the fluid composition. Metamorphic events are expressed as M1 (614–700 MPa), M2 (361–402 MPa), M3 (266–345 MPa) and M4 (150–193 MPa).

the CO_2-rich fluid inclusions at near-peak M2 conditions. As mentioned above, the nitrogen fugacity is calculated at 5.5 $\log_{10}$ units (Fig. 3) above the Cr-carlsbergite buffer (CCN + 5.5). Figure 6 is a diagram of pressure versus fluid composition for the COHN system for the same metamorphic P–T path (1 in Fig. 2) as used for the COH calculations. Figure 6 also shows the fluid molar volume and the temperature versus pressure. The molar fractions of H_2O, CO_2 and CH_4 in equilibrium with graphite do not significantly change in comparison with the COH system in Fig. 5. Between the M1 and M2 events, H_2O remains the predominant gas species in the fluid. The greatest concentrations of 64.1 and 59.8 mol% occur at 610.0 and 443.1 MPa respectively. The H_2O-rich fluid has a relatively low molar volume, between 32.5 and 37.1 $cm^3\,mol^{-1}$. CH_4 is the second most abundant gas species, varying between 15.2 and 45.9 mol% along this pressure trajectory. Sometime before the M2 event, CO_2 becomes the most abundant gas species and the molar volume increases drastically over a relatively short pressure interval to 50.5 $cm^3\,mol^{-1}$. If the CO_2 fraction were to reach a maximum of 95.0 mol% at 426.9 MPa, graphite would become unstable. As pressure decreases, the CO_2 fraction decreases and the N_2 fraction of the fluid increases. At 400.0 MPa (peak M2 metamorphic conditions) the fluid consists entirely of nitrogen, and has a molar volume of 53.1 $cm^3\,mol^{-1}$. Towards the lower pressure boundary of M2 at 378.6 MPa, CO_2 increases, and it again reaches a maximum of 95.1 mol% at 358.6 MPa with a peak molar volume of 54.0 $cm^3\,mol^{-1}$. At lower pressures the fluid is again in equilibrium with graphite. Between M2 and M3, H_2O increases to a maximum of 57.1 mol%, while the molar volume decreases drastically to 41.4 $cm^3\,mol^{-1}$. During and after M3, CH_4

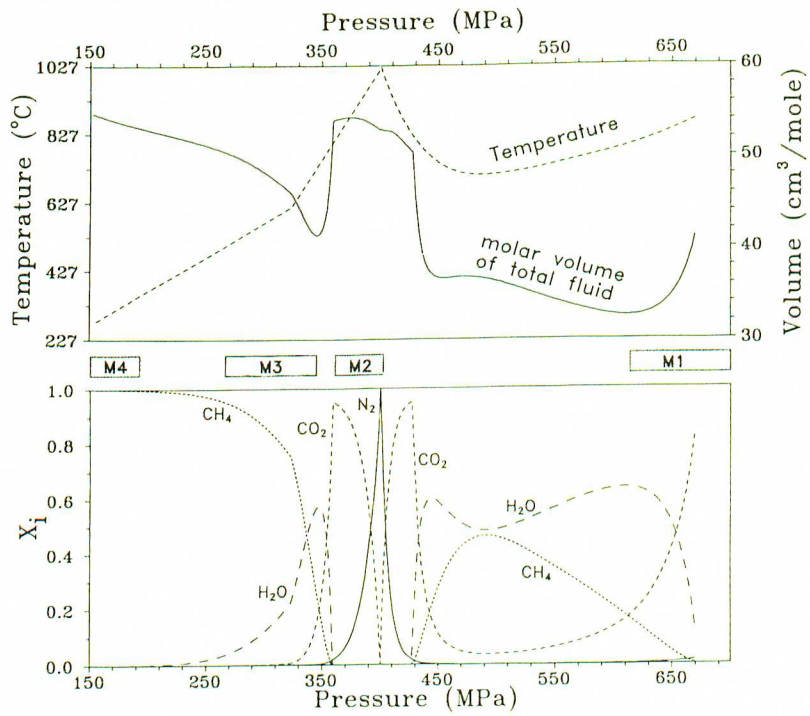

Fig. 6. Composite P–X_i (molar fraction of individual gas species) and combined P–T and P–V_M (molar volume) diagram. The main gas species are N_2 (solid line), CH_4 (stippled line), CO_2 (short-dashed line) and H_2O (long-dashed line). The P–T conditions used for fluid calculations correspond to path 1 in Fig. 2. The CCN buffer and the Ups60–Mt40 buffer (Fig. 3) are used as nitrogen and oxygen buffers, respectively (see text). The metamorphic events are expressed as M1 (614–700 MPa), M2 (361–402 MPa), M3 (266–345 MPa) and M4 (150–193 MPa).

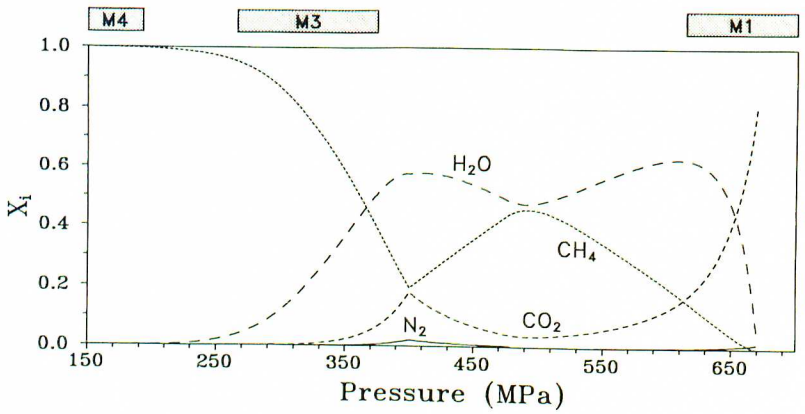

Fig. 7. P–X_i (mole fraction) diagram for the gas species N_2 (solid line), CH_4 (stippled line), CO_2 (short-dashed line) and H_2O (long-dashed line) when P–T path 2 (Fig. 2) is used for the calculations. The metamorphic events are expressed as M1 (614–700 MPa), M3 (266–375 MPa) and M4 (150–193 MPa).

becomes the dominant gas species in the fluid, while the molar volume increases continuously to 54.8 $cm^3\,mol^{-1}$ at 150 MPa.

To summarize, the most important features established from Fig. 6 are (1) the instability of graphite in fluids at peak metamorphic conditions (M2); (2) the occurrence of an H_2O-rich fluid between M1 and M2; (3) the relatively low molar volumes of these H_2O-rich fluids; (4) the absence of CH_4–N_2 fluids; (5) an N_2-rich fluid only coexists with CO_2 during M2; and (6) a CH_4-rich fluid develops after M3.

In addition, the fluid evolution has been calculated for rocks near the hypersthene-in isograd (path 2 in Fig. 2), which have lower M2 temperatures than path 1 (Fig. 7). Below 323 MPa and above 478 MPa, the fluid evolutions for both paths are similar. The increase in temperature between 323 and 478 MPa results in the fluid remaining H_2O-rich (48.8–57.7 mol%), which is then stable with graphite at all conditions. In this path, CH_4 and CO_2 are the second (19.5–44.5 mol%) and third (4.0–18.0 mol%) most abundant gas species, respectively (Fig. 7). Nitrogen remains a minor component (0.1–2.1 mol%).

In order to illustrate the similarity between our calculated fluid evolutions and those observed in natural fluid inclusions (Swanenberg, 1980; van den Kerkhof *et al.*, 1991), the patterns shown in Figs 5 & 6 may be redrawn in a CO_2–CH_4–N_2 diagram (Fig. 8). The open and closed symbols represent fluid inclusions with and without graphite, respectively. As previously mentioned, nitrogen may not be available in the rock system. Therefore, fluid compositions are proposed to occur between two end-values of the nitrogen buffer, zero (Fig. 5) and CCN + 5.5 (Fig. 6). Fluid compositions representative of the M1 and M3 events are shown by the shaded areas (Fig. 8), near the CO_2–CH_4 tie-line. The relative amount of N_2 in calculated CO_2–CH_4-rich fluids decreases towards the CH_4 apex. CO_2–N_2-rich M2 fluids are restricted to the tie-line between the pure phases and they do not contain graphite. Figure 8 indicates that the fluids in the central area and the CH_4–N_2-rich fluids do no correspond to any calculated compositions. The calculated fluid compositions, which are stable in the presence of graphite, correspond to the most frequently observed graphite-bearing fluid inclusions. The calculated molar volumes and the compositional evolution are represented in Fig. 9. The solid and open arrows in Fig. 9(a) indicate schematically the fluid development during M1, and in the period between M1 and M2, respectively. The solid arrow in Fig. 9(b) shows the compositional evolution of the fluid from M2 to M3. Corresponding molar volumes along both solid arrows are indicated. Although the fluids from M1 are identical in composition to those occurring between M2 and M3, their molar volumes are different. Observed molar volumes of natural fluid inclusions (Table 3) by van den Kerkhof *et al.* (1991) are grouped with nearly equal values in Fig. 9(c). Values at the CO_2–N_2 tie-line and along the CH_4 edge, enclosed in boxes, correspond to calculated molar volumes.

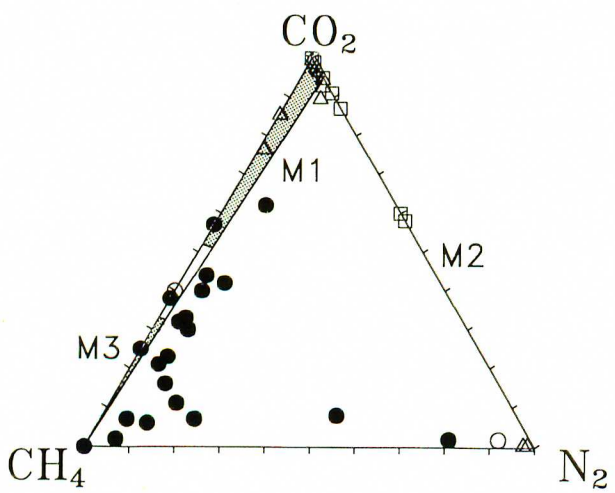

Fig. 8. CO_2–CH_4–N_2 composition diagram for M2 (CO_2–N_2 tie-line) and M1, M3 (shaded areas) events. Calculated fluid compositions along the CO_2–N_2 tie-line (M2) are not in equilibrium with graphite. All other calculated fluid compositions (M1, M3) are stable in the presence of graphite. Data from van den Kerkhof *et al.* (1991) are indicated with triangles (location A: Drangsdalen and Mydland), squares (location B: Faurefjell metasediments) and circles (location C: Austrumdalsvatnet). Closed and open symbols represent inclusions with graphite and without graphite, respectively.

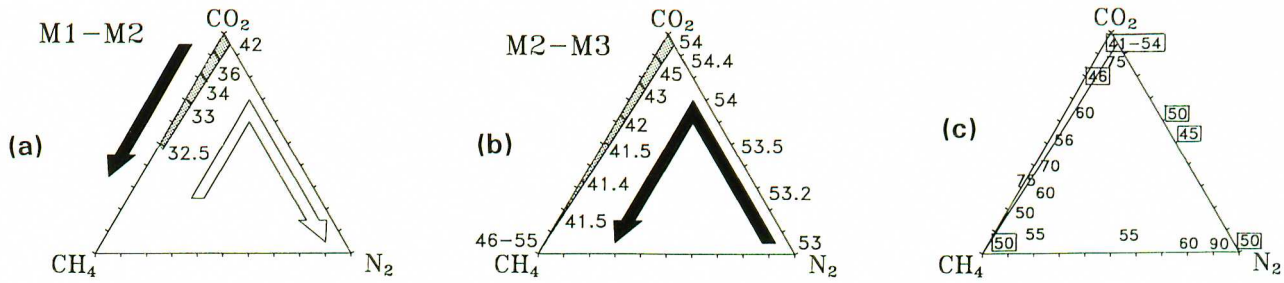

Fig. 9. CO_2–CH_4–N_2 composition diagrams with projected molar volumes ($cm^3\ mol^{-1}$). The calculated compositional evolution is schematically indicated with: (a) M1–M2, solid arrow during cooling of M1 and an open arrow for prograde changes from M1 to M2; (b) M2–M3, solid arrow for the post-M2 peak metamorphic episode towards M3 and M4—the shaded areas represent all possible compositions during the indicated fluid evolution; (c) measured values by van den Kerkhof *et al.* (1991)—values that correspond to calculated molar volumes are marked with rectangles.

DISCUSSION

The assumptions used in our calculations may lead to artefacts. Some measured natural fluid inclusions (Tables 2 & 3) fall outside the calculated range of fluid compositions and molar volumes (Figs 8 & 9c). Discrepancies are evident for CH_4–N_2-rich natural fluid inclusions and in the absence of H_2O from CO_2–CH_4-rich natural fluid inclusions with high molar volumes. Therefore, the assumptions must be scrutinized to test their validity.

Periods of deformation are likely to cause brittle strain in mineral grains, and cracking and crack-healing processes are consequently highly active during these periods. Therefore, we assume that crack healing occurs continuously during the long period of intense deformation (D2–D3), coeval with M2–M3 metamorphism.

The possibility that fluid inclusions trapped before peak metamorphic conditions of M2 are preserved must not be excluded (Samson & Williams-Jones, 1991). The recognition of M1 metamorphic mineral assemblages suggests that fluid inclusions formed during this metamorphic phase may be preserved. Swanenberg (1980) recognized CO_2-rich fluid inclusions with very low molar volumes ($36\ cm^3\ mol^{-1}$, Table 3). These must have formed from the calculated low-molar-volume CO_2-rich fluids of 35.6–$42.1\ cm^3\ mol^{-1}$ during M1 (Figs 6 & 9a).

Wilmart *et al.* (1991) describe CO_2–N_2 fluid inclusions with minor amounts of CH_4 in the Bjerkreim–Sokndal lopolith (Fig. 1), which corresponds with our calculated compositions for the enveloping metasediments of near-peak M2 temperatures. The calculated oxygen fugacity in the lopolith (Duchesne, 1970; Wilmart *et al.*, 1991) is approximately 1.5 $\log_{10}$ units higher than the enveloping metasediments (Jansen *et al.*, 1985). This fluid in the lopolith would remain rich in CO_2–N_2 during M3 according to our calculations. The absence of CH_4-rich fluid inclusions, which only occur at very low P–T conditions after M3, may result from scarcity of cracking and crack healing during this late stage of metamorphism and deformation. Based upon the occurrence of graphite in host minerals and in CO_2-rich fluid inclusions, Wilmart *et al.* (1991) concluded that the fluid system was closed between peak metamorphic conditions and 250° C, 200–300 MPa. Our calculated fluids fall within this range of conditions.

Iso-fugacities of oxygen and nitrogen are projected in a CO_2–CH_4–N_2 diagram for M1 conditions (865° C and 669 MPa, Fig. 10a) to indicate the fluid composition at the defined oxidation and nitrodation states. The oxygen fugacity, calculated with coexisting Fe–Ti oxides (Eq. 8), is $10^{-14.84}$ MPa, restricting the original fluid composition to the CO_2 apex of the diagram. Changes in fluid composition as a result of variation in oxygen and nitrogen fugacities can be immediately deduced from Fig. 10(a). Highly variable mineral assemblages on a millimetre scale indicate local equilibrium domains for M2 assemblages, suggesting a local oxygen fugacity control (Bol, 1990). Therefore, the oxidation state of the rock may deviate from that of the oxygen buffer used (Eq. 8). Recalculated fluid compositions, using an oxygen buffer one $\log_{10}$ unit lower than the previously mentioned buffer (Eq. 8), are shown in Fig. 11(a). Fluids richer in CH_4 are only produced during

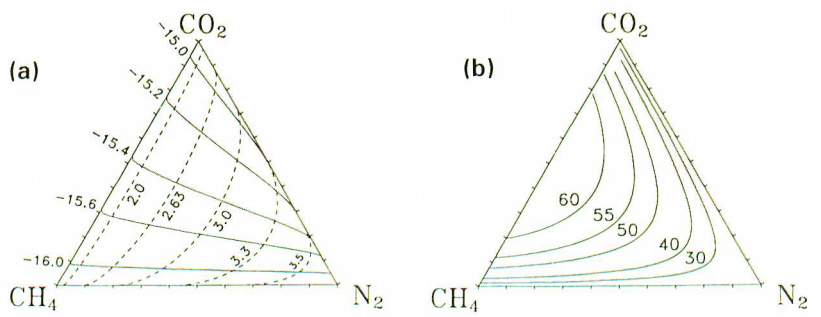

Fig. 10. CO_2–CH_4–N_2 diagrams for fluid compositions in equilibrium with graphite at M1 conditions: (a) iso-fugacity lines (in MPa) of oxygen (solid lines) and nitrogen (dashed lines), with values in $\log_{10}$ units; (b) H_2O isopleths (mol%), illustrating that the total amount of CO_2, CH_4 and N_2 may be a minor part of the fluid.

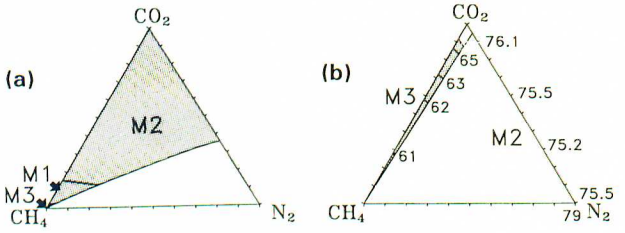

Fig. 11. (a) Calculated fluid composition for a mineral buffer with an O_2 fugacity one $\log_{10}$ unit lower than for coexisting Fe–Ti oxides (Eq. 8). Compositions in equilibrium with graphite during M2 (shaded area) in this case cover a larger part of the diagram than in Fig. 8. Both M1 and M3 are restricted to the CH_4 corner of the diagram. (b) Compositions and molar volumes ($cm^3\,mol^{-1}$) for an arbitrarily chosen $P_{fluid} = \frac{1}{2}P_{lithostatic}$. The shaded area covers all M3 compositions that are richer in CO_2 compared with those in Fig. 8. M2 fluids that are not in equilibrium with graphite are positioned at the CO_2–N_2 tie-line.

M1 and M3, while intermediate ternary compositions, which are not observed in natural fluid inclusions (Fig. 8), occur during M2. The calculations do not suggest CH_4–N_2-rich fluids, and therefore more reduced mineral buffers cannot clarify the existence of CH_4–N_2-rich fluid inclusions.

Dubessy *et al.* (1989) calculated fluids in the COHNS system. They used V–X properties of fluid inclusions measured at room conditions to estimate and to characterize the fluid at high P–T. This method differs from ours in which mineral equilibria are used to define oxygen and nitrogen fugacities at high P–T. Their method is only valid if the inclusions do not change in composition and density as a result of external factors. Dubessy *et al.* (1989) advocated the formation of N_2-rich fluid from NH_4^+-bearing minerals. It was proposed that the hydrogen derived from ammonium reacted to form CH_4, which then became the main carbon-bearing species. Therefore, the simultaneous occurrence of N_2 and CH_4 in fluid inclusions is assumed to be a stable fluid mixture. Our calculations indicate that CH_4–N_2-rich fluids may only occur at reducing conditions that are improbable ($f_{O_2} < 10^{-16}$ MPa in Fig. 10a) based upon the calculated oxygen fugacities from mineral assemblages in metasediments of Rogaland.

A trail of N_2-rich fluid inclusions, formed at peak M2 conditions, may be intersected by new cracks at a later stage, in the presence of a CH_4-rich fluid. Crack healing during this late stage would result in a new trail with CH_4-rich inclusions. Near the intersection, mixing of the two fluids may occur, producing CH_4–N_2 fluid inclusions. Swanenberg (1980) described the presence of such mixed H_2O–CO_2 inclusions at intersections of trails of H_2O- and CO_2-rich inclusions.

Fluid-deficient conditions have been proposed for several granulitic terranes. Lamb & Valley (1985) calculated a fluid pressure in the COH system of 100 MPa for a lithostatic pressure of 700 MPa, using an O_2 and an H_2O buffer, and proposed vapour-absent metamorphism. In order to model such circumstances here, fluid compositions and molar volumes have been calculated for an arbitrarily chosen fluid pressure of one-half the lithostatic pressure (Fig. 11b). Surprisingly, the compositions are identical to the originally calculated values (Fig. 8). M2 conditions remain on the CO_2–N_2 tie-line, but the upper boundary of M3 shifts towards the CO_2 apex and is responsible for most CO_2–CH_4-rich fluid inclusions. The high calculated molar volumes (Fig. 11b) correspond to data from some observed natural fluid inclusions (Tables 2 & 3, Fig. 9c).

The enigmatic CO_2–N_2-rich graphite-absent fluid inclusions from high-grade metasediments are thermodynamically stable at high temperature according to our calculations. The calculated graphite-absent compositions during M2, which lie along the CO_2–N_2 tie-line, are also found in natural fluid inclusions (Fig. 8). Furthermore, the calculated molar volumes, varying between 51.9 and 54.4 $cm^3\,mol^{-1}$, correspond to the measured values in natural fluid inclusions (Fig. 9c). The absence of graphite in fluid inclusions does not imply graphite was absent in the rock during entrapment.

A disadvantage of CO_2–CH_4–N_2 diagrams is that they do not represent complete fluid compositions. These three components may account for only a minor fraction of the fluid. Water isopleths of 30, 40, 50, 55 and 60 mol% are projected in Fig. 10(b) for M1 conditions, and demonstrate that H_2O is the major component for most fluids within the diagram. The calculated H_2O-rich fluid inclusions are positioned between CO_2 and CH_4 with minor amounts of N_2 (Fig. 8), coinciding with the gaseous CO_2–CH_4-rich metastable fluids in natural fluid inclusions (van den Kerkhof *et al.*, 1991).

Swanenberg (1980) did not identify H_2O-rich fluid inclusions pre-dating CO_2- and N_2-rich fluid inclusions, although H_2O-rich fluids occur in our calculations between M1 and M2 (Fig. 6). Such inclusions may have re-equilibrated completely because the presence of H_2O facilitates solution–precipitation and cracking mechanisms. Swanenberg (1980) assumed an H_2O-rich fluid during the M3 and M4 cycles following the CO_2- and N_2-rich fluid phases; this is supported by our calculations.

H_2O may be extracted from fluid inclusions after entrapment. Hollister (1988, 1990) argued for preferential leakage of H_2O from natural H_2O–CO_2-rich fluid inclusions, and Bakker & Jansen (1989, 1990, 1991b) have experimentally demonstrated this process. The effect of this process on the fluid composition in inclusions is clearly illustrated in COHN diagrams (Fig. 12). Point x in Fig. 12(a) represents the hypothetical original composition of an inclusion. Leakage of H_2O is indicated by the line xy (Fig. 12a). The composition is shifted towards y into the shaded area, where only metastable fluids exist. Chemical stability is then accomplished by precipitation of graphite, indicated by the line yz in Fig. 12(a), resulting from the reaction

$$CO_2 + CH_4 \rightarrow 2H_2O + 2C. \qquad (17)$$

This reaction was experimentally established in fluid inclusions by van den Kerkhof *et al.* (1991), the reaction being activated by energy from the Raman laser beam. Equilibrium is then reached for point z at the graphite

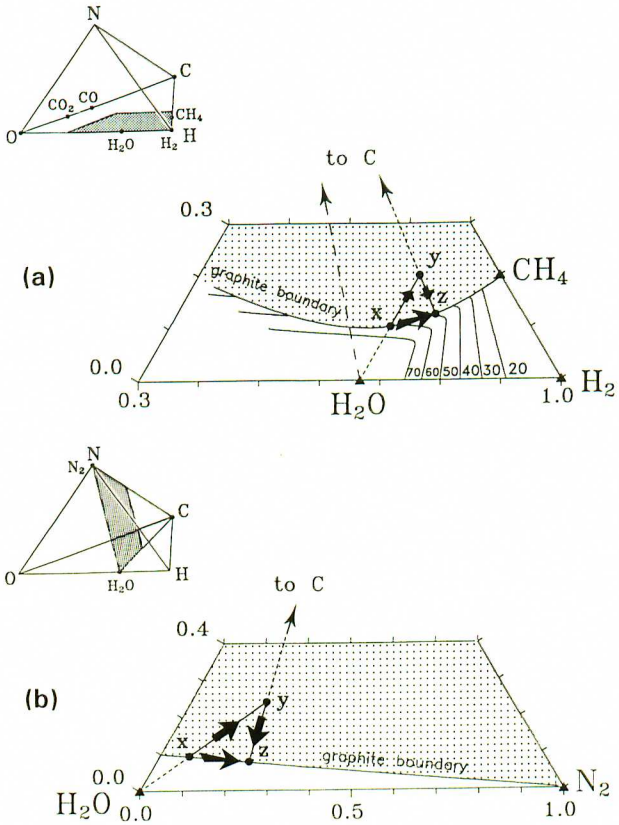

Fig. 12. Two sections of the COHN quadrangle for M1 conditions: (a) part of the COH diagram; (b) part of the C–N–H_2O diagram. The pure gas species are indicated with small triangles. The shaded areas in both diagrams represent metastable fluid compositions, the stable compositions are limited by the graphite boundary. The initial fluid composition x at the graphite boundary is arbitrarily chosen. Due to preferential H_2O leakage it shifts towards a metastable fluid y. Composition y shifts to a stable fluid z if graphite precipitates from the fluid (Eq. 17). If both processes occur simultaneously, the fluid composition x in fact moves along the graphite boundary to z.

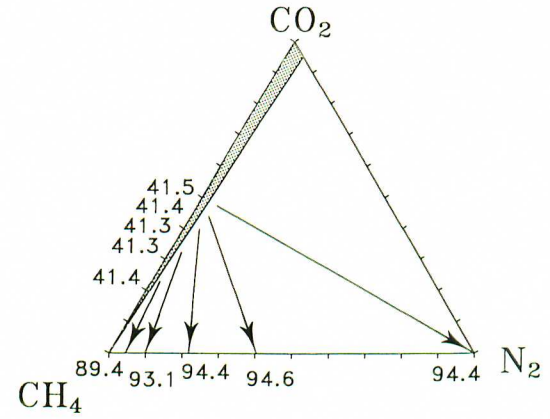

Fig. 13. CO_2–CH_4–N_2 composition diagram. The shaded area indicates all calculated fluid compositions, as in Fig. 8. The arrows show changes for stable fluids with small amounts of N_2 caused by preferential H_2O leakage and precipitation of graphite (Eq. 17). Increased molar volumes ($cm^3\,mol^{-1}$) are indicated with numbers.

boundary (Fig. 12a), which is richer in CH_4 at more reduced conditions. If preferential H_2O leakage and graphite precipitation occur simultaneously, fluid compositions will shift along the graphite boundary from x to z towards more CH_4-rich compositions. H_2O leakage would lead to inclusion compositions richer in CO_2 if the initial composition x is positioned at the graphite boundary left of the H_2O–carbon tie-line (large-dashed line in Fig. 12a).

Preferential H_2O leakage from inclusions with a low N_2 content is indicated in Fig. 12(b). As in Fig. 12(a), H_2O leakage is schematically illustrated with a composition change from x to y into the shaded area of metastable fluid compositions. Precipitation of graphite, towards a stable fluid composition at the graphite boundary, is indicated by the line yz (Fig. 12b). The fluid inclusions are relatively enriched in N_2. In the most extreme case, an inclusion with 63, 16, 16 and 2 mol% H_2O, CO_2, CH_4 and N_2 respectively (at 612.7 MPa and 791° C in Fig. 6) may contain only N_2 and solid graphite after leakage of all the H_2O. CO_2 and CH_4 available in equal amounts may then react completely to H_2O and graphite.

CH_4–N_2-rich fluids may develop by preferential H_2O leakage. The arrows in Fig. 13 indicate the compositional changes for CH_4-rich inclusions in a CO_2–CH_4–N_2 diagram after preferential H_2O leakage and precipitation of graphite (trajectory xz in Fig. 12). CH_4 was found by van den Kerkhof *et al.* (1991) to be the dominant fluid in inclusions from migmatites (Table 3). Depending on the initial composition and the amount of leakage, several observed natural CH_4–N_2-rich fluid inclusions (Fig. 8) might be representative of such compositional changes. If no gas reactions occur in the fluid inclusions after H_2O leakage, a metastable gas assemblage may then remain (trajectory xy in Fig. 12), corresponding to the observed high molar volumes of natural CO_2–CH_4-rich fluid inclusions. Their position in the CO_2–CH_4–N_2 diagram would not change. Graphite detected in natural fluid inclusions that have molar ratios of $CO_2/CH_4 < 0.6$ (van den Kerkhof *et al.*, 1991) may have precipitated after the entrapment, implying preferential H_2O leakage.

van den Kerkhof *et al.* (1991) proposed CH_4 to be the fluid generation following the CO_2–N_2-rich fluids. They assumed the post-entrapment formation of CH_4 in CO_2–N_2-rich fluid inclusions by H_2 diffusion, but did not exclude the possibility that CH_4 could be a product of retrograde cooling. Our calculations suggest that this must have been preceded by an H_2O-rich fluid (Fig. 6). The QFM buffer chosen by van den Kerkhof *et al.* (1991) to calculate equal CO_2/CH_4 ratios is too oxidizing and is therefore not realistic for the metamorphic rocks of Rogaland. Our calculations indicate the presence of a CH_4-rich fluid with minor amounts of H_2O occurring at the end of M3 and lower pressures for rocks within the pigeonite-in isograd.

The fluid evolution of rocks between the pigeonite-in and the orthopyroxene-in isograds (Fig. 1) is assumed to vary between the calculated evolutions at high peak M2

temperatures (Fig. 6) and low peak M2 temperatures (Fig. 7). The CO_2–N_2-rich fluid inclusions from location B (Fig. 1 and Faurefjell metasediments in Table 3), near the pigeonite-in isograd, correspond to the calculated fluid composition and molar volume at peak M2 conditions (Figs 6 & 9c). The composition of CO_2–N_2-rich fluid inclusions from location A (Fig. 1 and Drangsdalen in Table 3), near the pigeonite-in isograd, are similar to calculated compositions (Fig. 6). However, several measurements of molar volume of nearly pure N_2 and CO_2 fluid inclusions are too high, indicating possible post-entrapment re-equilibration through volume adjustments. Fluid inclusions from location C (Fig. 1 and Austrumdalsvatnet in Table 3) are CH_4–N_2-rich and CH_4–CO-rich. Graphite is present, and H_2O is occasionally absent in these inclusions. These rocks are located further from the intrusive complex, and nearer to the orthopyroxene-in isograd (Fig. 1). Therefore, the natural fluid must resemble the calculated fluid in Fig. 7, in which H_2O is the most abundant and CH_4 the second most abundant gas species. The high molar fraction of H_2O would cause fluid inclusions easily to re-equilibrate by preferential leakage of H_2O, and by possible volume adjustments. A metastable gas mixture remains that has more than 50 mol% CH_4, or this gas mixture reacts to more stable CH_4–N_2-rich compositions, implying precipitation of graphite in the fluid inclusions.

CONCLUSIONS

Information regarding mineral assemblages, timing of metamorphic or magmatic events, deformation phases and oxidation/nitrodation state in metamorphic rocks can be used to calculate fluid evolutions with corresponding compositions and molar volumes.

Although only scarce thermodynamic information is available for natural N-bearing minerals, the Cr-carlsbergite buffer (Eq. 16) can be successfully used to indicate the N_2 fugacity of the rock, analogous to the method for O_2 fugacity described by Holloway (1981).

Natural fluid inclusions recorded in rocks from Rogaland (Swanenberg, 1980; van den Kerkhof *et al.*, 1991) correspond partly with calculated compositions and molar volumes of fluids based on a P–T path, oxygen and nitrogen buffer, as exemplified by (1) the absence of graphite in CO_2–N_2-rich fluid inclusions, (2) the absence of intermediate ternary CO_2–CH_4–N_2 compositions, (3) high-density CO_2-rich fluid inclusions (36–42 $cm^3\,mol^{-1}$), (4) CO_2–CH_4-rich fluid inclusions with minor amounts of N_2 (up to 5 mol%) during M2–M3.

The existence of CH_4–N_2-rich fluid inclusions can be explained by preferential H_2O leakage (the remnant unstable composition subsequently reacting to a stable CH_4–N_2-rich fluid) or by mixing of intersecting trails of N_2- and CH_4-rich fluid inclusions, not but by introducing more reduced fluids into the system, nor by assuming fluid-deficient conditions.

High-molar-volume CO_2–CH_4-rich fluid inclusions with low molar fractions of H_2O are unstable at M2–M3 conditions and must have resulted from preferential H_2O leakage.

Post-entrapment alteration, which is proposed by van den Kerkhof *et al.* (1991) to explain their measured gaseous fluids, must have affected mainly H_2O-rich fluid inclusions.

ACKNOWLEDGEMENTS

We thank L. S. Hollister, A. M. van den Kerkhof, R. D. McDonnell, R. D. Schuiling and J. L. R. Touret for discussion. This work was funded by Stichting Aardwetenschappelijk Onderzoek Nederland (AWON/NWO).

REFERENCES

Arrhenius, G., 1950. Carbon and nitrogen in subaquatic sediments. *Geochimica et Cosmochimica Acta*, **1**, 15–21.

Bakker, R. J., 1992. The programs COHN: theoretical background and program structure. *Geologica Ultraiectina*, **94**, 97–133.

Bakker, R. J. & Jansen, J. B. H., 1989. Experimental evidence for leakage of H_2O from CO_2–H_2O rich fluid inclusions. *Terra Abstracts*, **1**, 380.

Bakker, R. J. & Jansen, J. B. H., 1990. Preferential water leakage from fluid inclusions by means of mobile dislocations. *Nature*, **345**, 58–60.

Bakker, R. J. & Jansen, J. B. H., 1991a. Stability of CO_2–CH_4–N_2 rich fluid inclusions. *Plinius*, **5**, 11–13.

Bakker, R. J. & Jansen, J. B. H., 1991b. Experimental post-entrapment water loss from synthetic CO_2–H_2O inclusions in natural quartz. *Geochimica et Cosmochimica Acta*, **55**, 2215–2230.

Bastoul, A., Pironon, J. & Cuney, M., 1991. Nitrogen geochemistry in metamorphic fluids and minerals from a Raman and micro FT-IR study. The example of the Central Jebilets, Morocco. *Plinius*, **5**, 16.

Berman, R. G., 1988. Internally-consistent thermodynamic data for minerals in the system Na_2O–K_2O–CaO–MgO–FeO–Fe_2O_3–Al_2O_3–SiO_2—TiO_2–H_2O–CO_2. *Journal of Petrology*, **29**, 445–522.

Bol, L. C. G. M., 1990. Geochemistry of high-temperature granulitic supracrustals from Rogaland, SW Norway. *Geologica Ultraiectina*, **66**, 1–137.

Bos, A., 1990. Hydrothermal element distributions at high temperatures. *Geologica Ultraiectina*, **69**, 1–99.

Bos, A., Duit, W., Van den Eerden, A. M. J. & Jansen, J. B. H., 1988. Nitrogen storage in biotite: an experimental study of the ammonium and potassium partitioning between 1M-phlogopite and vapour at 2 kb. *Geochimica et Cosmochimica Acta*, **52**, 1275–1283.

Buddington, A. F. & Lindsey, D. H., 1964. Iron–titanium oxide minerals and synthetic equivalents. *Journal of Petrology*, **5**, 310–357.

Dhamelincourt, P., Bény, J. M., Dubessy, J. & Poty, B., 1979. Analyse d'inclusions fluides á la microsonde MOLE á effet Raman. *Bulletin de Minéralolgie*, **102**, 600–610.

Doria, A., Boiron, M. C. & Noronha, F., 1991. Metamorphic fluids in quartz veins and their surroundings. An example of an Au-district of Northern Portugal. *Plinius*, **5**, 60.

Dubessy, J. & Ramboz, C., 1986. The history of organic nitrogen from early diagenesis to amphibolite facies: mineralogical, chemical, mechanical and isotopic consequences. In: *Fifth Int. Symp. on Water–Rock Interaction*, pp. 1771–1774.

Dubessy, J., Poty, B. & Ramboz, C., 1989. Advances in C–O–H–N–S fluid geochemistry based on micro-Raman spectrometric analysis of fluid inclusions. *European Journal of Mineralogy*, **1**, 517–534.

Duchesne, J. C., 1970. Iron–titanite oxide minerals in the Bjerkrem-Sogndal Massif, South-western Norway. *Journal of Petrology*, **13,** 57–81.

Duchesne, J. C., Maquil, R. & Demaiffe, D., 1985. The Rogaland anorthosites: facts and speculations. In: *The Deep Proterozoic Crust in the North Atlantic Provinces* (eds Tobi, A. C. & Touret, J. L. R.), pp. 449–476. Reidel, Dordrecht.

Duit, W., Jansen, J. H. B., Van Breemen, A. & Bos, A., 1986. Ammonium micas in metamorphic rocks as exemplified by Dome de l'Agout (France). *American Journal of Science*, **286,** 702–732.

Eugster, H. P. & Skippen, G. B., 1967. Igneous and metamorphic reactions involving gas equilibria. In: *Researches in Geochemistry*, Vol. 2 (ed. Abelson, P. H.), pp. 492–520. J. Wiley, London.

Ferry, J. M., 1979. A map of chemical potential differences within an outcrop. *American Mineralogist*, **64,** 966–985.

Ferry, J. M. & Burt, D. M., 1982. Characterization of metamorphic fluid composition through mineral equilibria. In: *Characterization of Metamorphism Through Mineral Equilibria. Reviews in Mineralogy*, Vol. 10 (ed. Ferry, J. M.), pp. 207–262.

Flowers, G. C., 1979. Correction of Holloway's (1977) adaption of the modified Redlich–Kwong equation of state for calculation of the fugacities of molecular species in supercritical fluids of geological interest. *Contributions to Mineralogy and Petrology*, **69,** 315–318.

French, B. M., 1966. Some geological implications of equilibrium between graphite and a C–H–O gas phase at high temperatures and pressures. *Reviews of Geophysics*, **4,** 223–253.

Frost, B. R. & Chacko, T., 1989. The granulite uncertainty principle: limitations on thermometry in granulites. *Journal of Geology*, **97,** 435–450.

Greenwood, H. J., 1975. Buffering of pore fluids by metamorphic reactions. *American Journal of Science*, **275,** 573–593.

Guilhaumou, N., Dhamelincourt, P., Touray, J-C. & Touret, J., 1981. Etude des inclusions fluides du systeme N_2–CO_2 de dolomites et de quartz de Tunesie septentrionale. Donnees de la microcryoscopie et de l'analyse a la microsonde a effet Raman. *Geochimica et Cosmochimica Acta*, **45,** 657–673.

Heggerty, S. E., 1976. Opaque mineral oxides in terrestrial igneous rocks. In: *Oxide Minerals. Reviews in Mineralogy*, Vol. 3 (ed. Rumble, D., III), pp. Hg101–Hg175.

Hall, D. L., Sterner, S. M. & Bodnar, R. J., 1989. Experimental evidence for hydrogen diffusion into fluid inclusions in quartz. *Geological Society of America Abstracts with Programs*, **21,** A358.

Hallam, M. & Eugster, H. P., 1976. Ammonium silicate stability relations. *Contributions to Mineralogy and Petrology*, **57,** 227–234.

Hansen, E. C., Newton, R. C. & Janardhan, A. S., 1984. Fluid inclusions in rocks from the amphibolite-facies gneiss to charnockite progression in southern Karnataka, India: direct evidence concerning the fluids of granulite metamorphism. *Journal of Metamorphic Geology*, **2,** 249–264.

Hermans, G. A. E. M., Tobi, A. C., Poorter, R. P. E. & Maijer, C., 1975. The high-grade metamorphic Precambrian of the Sirdal–Orsdal Area, Rogaland/Vest-Agder, South-west Norway. *Norges Geologiske Undersøkelse*, **318,** 51–74.

Hollister, L. S., 1988. On the origin of CO_2-rich fluid inclusions in migmatites. *Journal of Metamorphic Geology*, **6,** 467–474.

Hollister, L. S., 1990. Enrichment of CO_2 in fluid inclusions in quartz by removal of H_2O during crystal-plastic deformation. *Journal of Structural Geology*, **12,** 895–901.

Holloway, J. R., 1977. Fugacity and activity of molecular species in supercritical fluids. In: *Thermodynamics in Geology* (ed. Fraser, D. G.), pp. 161–182. Reidel, Dordrecht.

Holloway, J. R., 1981. Compositions and volumes of supercritical fluids in the Earth's crust. In: *Short Course in Fluid Inclusions: Applications to Petrology*, Vol. 6 (eds Hollister, L. S. & Crawford, M. L.), pp. 13–38. Mineralogical Association of Canada.

Holloway, J. R. & Reese, R. L., 1974. The generation of N_2–CO_2–H_2O fluids for use in hydrothermal experimentation 1. Experimental method and equilibrium calculations in the C–O–H–N system. *American Mineralogist*, **59,** 587–597.

Honma, H. & Itihara, Y., 1981. Distribution of ammonium in minerals of metamorphic and granitic rocks. *Geochimica et Cosmochimica Acta*, **45,** 983–988.

Huijsmans, J. P. P., Kabel, A. B. E. T. & Steenstra, S. E., 1981. On the structure of a high-grade metamorphic Precambrian terrain in Rogaland, south Norway. *Norsk Geologisk Tidsskrift*, **61,** 183–192.

Jacobs, G. K. & Kerrick, D. M., 1981. Methane: an equation of state with application to the ternary system H_2O–CO_2–CH_4. *Geochimica et Cosmochimica Acta*, **45,** 607–614.

JANAF (1971). *Thermochemical Tables*. National Bureau of Standards.

Jansen, J. B. H., Blok, R. J. P., Bos, A. & Scheelings, M., 1985. Geothermometry and geobarometry in Rogaland and preliminary results from the Bamble Area, S. Norway. In: *The Deep Proterozoic Crust in the North Atlantic Provinces* (eds Tobi, A. C. & Touret, J. L. R.), pp. 499–516. Reidel, Dordrecht.

Lamb, W. M. & Valley, J. W., 1985. C–O–H fluid calculations and granulite genesis. In: *The Deep Proterozoic Crust in the North Atlantic Provinces* (eds Tobi, A. C. & Touret, J. L. R.), pp. 119–131. Reidel, Dordrecht.

van den Kerkhof, A. M., Touret, J. L. R., Maijer, C. & Jansen, J. B. H., 1991. Retrograde methane-dominated fluid inclusions from high-temperature granulites of Rogaland, southwestern Norway. *Geochimica et Cosmochimica Acta*, **55,** 2533–2544.

Kerrick, D. M. & Jacobs, G. K., 1981. A modified Redlich–Kwong equation for H_2O, CO_2, and H_2O–CO_2 mixtures at elevated pressures and temperatures. *American Journal of Science*, **281,** 735–767.

Maijer, C. & Padget, P. (eds) 1987. The geology of the southernmost Norway: an excursion guide. *Norges Geologiske Undersøkelse Special Publication*, **1**.

Pasteels, P., Demaiffe, D. & Michot, J., 1979. U–Pb and Rb–Sr geochronology of the eastern part of the south Rogaland igneous complex, S. Norway. *Lithos*, **12,** 199–208.

Rice, J. M. & Ferry, J. M., 1982. Buffering, infiltration, and the control of intensive variables during metamorphism. In: *Characterization of Metamorphism Through Mineral Equilibria. Reviews in Mineralogy*, Vol. 10 (ed. Ferry, J. M.), pp 207–262.

Robie, R. A., Hemingway, B. S. & Fisher, J. R., 1978. Thermodynamical properties of minerals and related substances at 298.15 K and 1 bar (10^5 Pascals) pressure and at higher temperatures. *United States Geological Survey Bulletin*, **1452,** 1–455.

Samson, I. M. & Williams-Jones, A. E., 1981. C–O–H–N-salt fluids associated with contact metamorphism, McGerrigle Mountains, Quebec: a Raman spectroscopic study. *Geochimica et Cosmochimica Acta*, **55,** 169–177.

Sauter, P. C. C., 1983. Metamorphism of siliceous dolomites in the high grade Precambrium of Rogaland, SW Norway. *Geologica Ultraiectina*, **32,** 1–143.

Saxena, S. K., 1989. Oxidation state of the mantle. *Geochimica et Cosmochimica Acta*, **53,** 89–95.

Saxena, S. K. & Fei, Y., 1987. Fluids at crustal pressure and temperatures. *Contributions to Mineralogy and Petrology*, **95,** 370–375.

Skippen, G. B. & Marshall, D. D., 1991. The metamorphism of granulites and devolatization of the lithosphere. *Canadian Mineralogist*, **29,** 693–705.

Spencer, K. J. & Lindsey, D. H., 1981. A solution model for coexisting iron–titanium oxides. *American Mineralogist*, **66,** 1189–1201.

Stevenson, F. J., 1962. Chemical state of the nitrogen in rocks. *Geochimica et Cosmochimica Acta*, **26,** 797–809.

Swanenberg, H. E. C., 1980. Fluid inclusions in high-grade metamorphic rocks from SW Norway. *Geologica Ultraiectina*, **25,** 1–147.

Thompson, A. B., 1975. Mineral reactions in a calc-mica schist from Gassetts, Vermont, USA. *Contributions to Mineralogy and Petrology*, **53,** 105–127.

Thompson, J. B. & Thompson, A. B., 1976. A model system for mineral assemblages in pelitic schists. *Contributions to Mineralogy and Petrology*, **58,** 243–277.

Tobi, A. C., Hermans, G. A. E. M., Maijer, C. & Jansen, J. B. H., 1985. Metamorphic zoning in the high-grade proterozoic of Rogaland–Vest Adger, SW Norway. In: *The Deep Proterozoic Crust in the North Atlantic Provinces* (eds Tobi, A. C. & Touret, J. L. R.), pp. 477–497. Reidel, Dordrecht.

Touret, J., 1982. An empirical phase diagram for a part of the N_2–CO_2 system at low temperatures. *Chemical Geology*, **37,** 49–58.

Ulmer, G. C., Grandstaff, D. E., Weiss, D., Moats, M. A., Buntin, T. J., Gold, D. P., Hatton, C. S., Kadik, A., Koseluk, R. A. & Rosenhauer, M., 1987. The mantle redox state: an unfinished story? *Geological Society of America Special Paper*, **215,** 5–23.

Valley, J. W., Bohlen, S. R., Essene, E. J. & Lamb, W., 1990. Metamorphism in Adirondacks: II. The role of fluids. *Journal of Petrology*, **31,** 555–596.

Voncken, J. H. L., Konings, R. J. M., Jansen, J. B. H. & Woensdrecht, C. F., 1988. Hydrothermally grown buddingtonite, an anhydrous ammonium feldspar ($NH_4AlSi_3O_8$). *Physics and Chemistry of Minerals*, **15,** 323–328.

Wielens, J. B. W., Andriessen, P. A. M., Boelrijk, N. A. I. M., Hebeda, E. H., Priem, H. N. A., Verdurmen, E. A. & Verschure, R. H., 1981. Isotope geochronology in the high-grade metamorphic Precambrian of southwestern Norway: new data and reinterpretations. *Norges Geologiske Undersøkelse*, **359,** 1–30.

Wilmart, E., Clocchiatti, R., Duchesne, J. C. & Touret, J. L. R., 1991. Fluid inclusions in charnockites from the Bjerkreim–Sokndal massif (Rogaland, southwestern Norway): fluid origin and in situ evolution. *Contributions to Mineralogy and Petrology*, **108,** 453–462.

Received 5 March 1992; revision accepted 12 October 1992.